Design of a Portable Photovoltaic *I–V* Curve Tracer Based on the DC–DC Converter Method

Thiago A. Pereira ⓘ, Lenon Schmitz ⓘ, *Student Member, IEEE*, Walbermark M. dos Santos ⓘ,
Denizar C. Martins ⓘ, *Senior Member, IEEE*, and Roberto F. Coelho ⓘ, *Member, IEEE*

Abstract—The *I–V* curve tracer is an instrument that captures the current–voltage characteristics of photovoltaic (PV) generators under real operating conditions. Such device can be used to evaluate their performance and identify faults or aging effects, but its high costs have prevented it from being widely used in the industry. This article thus proposes the design of a low-cost, portable *I–V* curve tracer based on the classic dc–dc Ćuk converter for PV modules of up to 300 W. In order to obtain a compact device, some design techniques are proposed, including circuit reduction, high switching frequency operation, specification of the optimum load resistor power rating, and improved measurement distribution because of a nonlinear duty cycle variation. Experimental curves were compared with those acquired from commercial PV tracers to demonstrate its accuracy. In addition, the physical parameters of the well-known single-diode model have been extracted and compared with data provided by manufacturers to identify aging effects and module performance.

Index Terms—Ćuk converter, *I–V* curve tracer, photovoltaic (PV) module performance, real operating conditions.

I. INTRODUCTION

PHOTOVOLTAIC (PV) generators are characterized by nonlinear curves called *I–V* (current *versus* voltage) and *P–V* (power *versus* voltage) curves [1]. Instead of being fixed, these curves change according to the climate conditions: solar irradiance (G) and temperature (T), implying variations on voltage, current, and power provided by PV generators [2]. The knowledge of these curves plays an important role in installation, commissioning, and maintenance of PV systems [3]–[6]. However, the information contained in manufacturer datasheets usually targets the PV electrical variables for two operating points: standard test conditions (STC) and nominal operating temperature cell. Therefore, when required for any other weather condition, the *I–V* and *P–V* curves need to be measured or extrapolated from numerical models [7], [8].

The principle for obtaining the experimental *I–V* and *P–V* curves consists on monitoring the current supplied by the PV module for a complete excursion of the voltage applied across its terminals, from zero up to the open-circuit voltage, or vice-versa. For this purpose, there are different methods proposed in the technical literature, such as the variable resistive load, the capacitive load, the electronic load, and the dc–dc converter methods [9], [10].

The simplest method to measure the *I–V* curve is based on the usage of a variable resistor across the PV generator terminals, normally achieved by an array of resistors that can be alternately connected and disconnected by active switches [11]–[14]. However, to cover the entire *I–V* curves, the resistor bank is generally bulky and hard to be adjusted so that the measurement points are distributed evenly along the *I–V* curve. Moreover, by using this method the measurement range is often limited by the larger equivalent resistance so that the gap between the maximum measured point and the open-circuit voltage point can be very large [10].

The capacitive method applies a capacitor directly to the PV generator [15]–[21]. As the charge of the capacitor increases, the voltage on the capacitor terminals gradually rises and the current decreases. If these variables were stored during a complete charge or discharge cycle, the *I–V* curves might be easily plotted. Nonetheless, high-quality capacitors are required to reliably measure different *I–V* curves. Such capacitors should cover a large range of capacitance, voltage, and inrush current, which may result in large size and high costs. Additionally, the measuring time is highly dependent on the PV parameters and the capacitors charging behavior [9].

The electronic load method uses a transistor (typically a MOSFET) as the load of the PV generator [22]–[27]. The drain-source ON-state resistance is modulated to increase the PV output current from zero up to the short-circuit value, while the voltage varies from the open-circuit voltage up to zero. In this method, the energy delivered by the PV generator is consumed by the transistor instead of a resistor. Therefore, a heatsink might be necessary to maintain its operating junction temperature within the recommended limits. When needed, the heatsink makes the device heavy and bulky, limiting its application [10].

Finally, the dc–dc converter method allows the variation of the equivalent resistance seen by the PV generator by acting on the duty cycle of a dc–dc converter connected to its terminals [28]–[35]. Although the dc–dc converter method may demand a larger number of components to assemble its control and power

stages, it is highly efficient and low in cost. However, because of the high switching frequency, the system is subjected to noise, demanding more attention on the data acquisition. According to [9] and [10], the dc–dc converter tracing method has the best performance when considering the accuracy, sweep speed, maximum rating, and resolution, compared with its counterparts. Additionally, it could represent a future trend in *I–V* curve tracers, since control strategies can be added to obtain more stable and accurate measurements, but to meet market expectations, more progress is required to reduce volume and cost [10].

Currently, according to our investigation, the capacitive load method is the most used in commercial *I–V* tracers. In addition, although the dc–dc converter method has the best performance, the most portable PV tracers use the capacitive load method because it is easy to be compacted [10]. In light of this, the presented article proposes the design of a portable *I–V* tracer for PV modules of up to 300 W based on the classic dc–dc Ćuk converter. In order to obtain a compact device, some design techniques are implemented, as the operation at high switching frequency, reducing the size of passive components, and a circuit reduction by eliminating the output capacitor from the conventional Ćuk converter. Additionally, two original contributions are proposed: 1) a simple methodology to design the optimum load resistor power rating based on the integral-cycle control (ICC) principle for sequential measurements; and 2) nonlinear variation of duty cycle to improve the distribution of the measurements along the *I–V* curve, which also reduces the temperature rise in the load resistor.

In the proposed PV tracer, values of current, voltage, irradiance, and temperature are measured, conditioned, accumulated and thus, transferred to a computer, allowing the determination of the five parameters of the classical single-diode model. In the possession of those parameters it is possible to replicate the module behavior in offline simulation platforms under different conditions of temperature and irradiance. Since the shape of these curves can provide information about any impairment that reduces its power (including damaged cells, short-circuit bypass diodes, local shading, module mismatch, increased shunt or series resistance), the obtained results are also compared with the curves provided by the manufacturers in order to identify device degradation and aging effects.

II. DC–DC Converters as Variable Resistances

The dc–dc converter method consists in varying the voltage on the PV generator terminals (from zero to the open-circuit value) by controlling the duty cycle D applied to the dc–dc converter employed as *I–V* curve tracer, as illustrated in Fig. 1(a). Independently of the selected dc–dc converter, its output and input voltages can be related by its static gain M

$$V_o = MV_{\text{pv}}. \tag{1}$$

Moreover, according to the law of conservation of energy, the power supplied by the PV generator is equal to the power consumed by the load

$$V_{\text{pv}}I_{\text{pv}} = \frac{V_o^2}{R_o}. \tag{2}$$
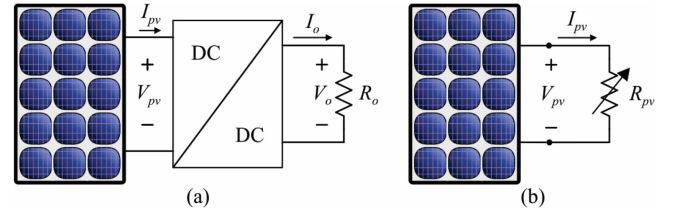

Fig. 1. (a) PV generator connected to a load resistor through a dc–dc converter. (b) Equivalent input resistance seen by the PV generator terminals.

TABLE I
EQUIVALENT RESISTANCE OF BASIC DC–DC CONVERTERS

dc-dc converter	static gain (M)	equivalent resistance (R_{pv})	$R_{pv,max}$	$R_{pv,min}$
Buck	D	$\dfrac{R_o}{D^2}$	∞	R_o
Boost	$\dfrac{1}{1-D}$	$(1-D)^2 R_o$	R_o	0
Buck-boost, Ćuk, SEPIC, and Zeta	$\dfrac{D}{1-D}$	$\dfrac{(1-D)^2 R_o}{D^2}$	∞	0

Thus, substituting (1) in (2), yields to

$$R_{\text{pv}} = \frac{V_{\text{pv}}}{I_{\text{pv}}} = \frac{R_o}{M^2}. \tag{3}$$

Equation (3) allows understanding the dc–dc converter as a variable resistance, as shown in Fig. 1(b), whose value depends on the load resistance R_o and the static gain M of the power converter. The static gains M of the basic dc–dc converters are presented in Table I, considering the operation in continuous conduction mode (CCM). As can be noted, in CCM these static gains are only dependent on the duty cycle D, which is ideally limited in the range of [0, 1]. This means that R_{pv} is also restricted to the ranges specified in Table I. To completely sweep an *I–V* curve, the emulated resistance R_{pv} needs to vary from infinite to zero. Therefore, according to Table I, only the buck–boost, Ćuk, SEPIC, and Zeta converters are able to satisfy this condition [36], [37]. The buck converter is not able to measure the points of the curve close to the short-circuit (I_{sc}) current, whereas the boost converter cannot measure the points in the vicinity of the open-circuit voltage (V_{oc}).

III. Proposed Photovoltaic *I–V* Curve Tracer

The proposed PV *I–V* curve tracer is depicted in Fig. 2 by a simplified block diagram. Such a device was designed for PV modules of up to 300 W and maximum values of open-circuit voltage and short-circuit current of 50 V and 10 A. In general, it can be divided in three basic parts: the power converter, the control strategy, and the data acquisition system.
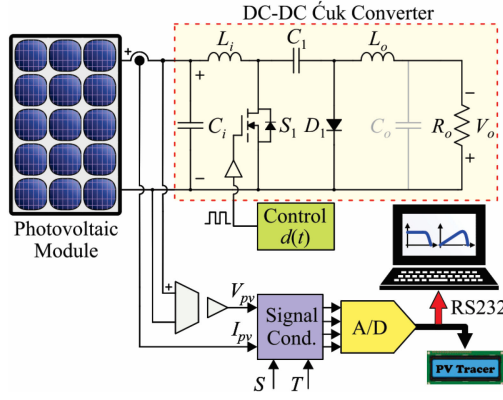
Fig. 2. Simplified diagram of the PV tracer based on the dc–dc Ćuk converter.

TABLE II
MAXIMUM RIPPLES IN THE PASSIVE COMPONENTS

Switching frequency $- f_s$	100 kHz
Maximum input current ripple $- \Delta I_i$	20%
Maximum input voltage ripple $- \Delta V_i$	2%
Maximum output current ripple $- \Delta I_o$	20%
Maximum voltage ripple at $C_1 - \Delta V_{C1}$	20%

A. Power Converter

Among the four-basic dc–dc topologies that can measure the entire I–V curve, the Ćuk converter is the simplest one with input current source feature. Since this behavior is desirable to avoid high current ripple in the PV module, this converter is selected for the proposed application.

Taking into account that the main role of its output capacitor C_o is providing a path of low impedance for the output current in the switching frequency, and considering that the PV curve tracer only requires measurements of the input quantities ($V_{\rm pv}$ and $I_{\rm pv}$), high-frequency components flowing through the load is not a problem. Therefore, in the proposed application the output capacitor is suppressed for the purpose of helping the device volume reduction. Additionally, in order to achieve a portable device, the Ćuk converter has been designed to operate with a high switching frequency f_s of 100 kHz, reducing the size of the remaining passive elements. Table II summarizes the ripple specifications used to design these passive elements, which were calculated by the following:

$$L_i = \frac{R_{\rm mp}D}{f_s\Delta I_i} \tag{4}$$

$$L_o = \frac{MR_{mp}D}{f_s\Delta I_o} \tag{5}$$

$$C_1 = \frac{D(1-D)}{f_s\Delta V_{C1}R_{mp}M} \tag{6}$$

$$C_i = \frac{4\Delta I_i}{\pi^3 f_s\Delta V_i} \tag{7}$$

TABLE III
SUMMARIES OF THE COMPONENT VALUES OF THE ĆUK CONVERTER

Input capacitor $- C_i$	4.7 μF / 100 V
Input inductor $- L_i$	158.6 μH / APH23P60
Capacitor Ćuk $- C_1$	1.0 μF / 250 V
Output inductor $- L_o$	326.8 μH / APH23P60
Load resistor $- R_o$	20 Ω / 30 W
MOSFET $- S_1$	IPD35N10S3L-26
Diode $- D_1$	MBRD20200CT
Gate driver	UCC37324D
Microcontroller (CPU)	Atmega328P $-$ 8 bits
Current Sensor	ACS724-10 UT
Voltage Sensor	Resistive divider

where

$$D = \frac{M}{M+1} \tag{8}$$

$$M = \sqrt{\frac{R_o}{R_{mp}}} \tag{9}$$

$$R_{mp} = \frac{V_{mp}}{I_{mp}}. \tag{10}$$

The passive elements were designed for the Ćuk converter operating at its worst scenario, supposedly a PV module in its maximum power point at STC. For silicon-based PV modules of 60–72 cells at STC, R_{mp} is typically between 3–5 Ω, resulting in the components listed in Table III. Moreover, Table III also presents the semiconductor devices used in the proposed PV tracer. Such devices were selected considering the worst current and voltage stresses that can arise, following conventional procedures for the Ćuk converter, as realized in [38]–[40].

B. Control Strategy

The I–V curve is swept through the converter duty cycle. The sweep time interval t_{sp} plays an important role in the quality of the obtained curves and has to be carefully selected. It should be small enough to ensure that the readings of voltage and current are accomplished under constant solar irradiance and temperature, but large enough to ensure they are in steady-state during the readings.

Because of the thermal inertia, the PV generator temperature varies slowly, with typical rates of 1°C/min. Furthermore, in sunny days without clouds, the dynamics associated with the irradiance is also slow, typically lower than 300 Wm^{-2}/h on the summer [41], [42]. Even during partially cloudy days, when the irradiance oscillations become more pronounced, the variations occur in intervals of seconds, or, rarely, in hundreds of milliseconds. Moreover, the transient response of the designed Ćuk converter typically takes less than one millisecond to reach the steady-state for small variations in the duty cycle. Therefore, in order to avoid irradiance and temperature changes during the data acquisition and, at the same time, to ensure that the Ćuk converter is in steady-state during the readings, the sweep time
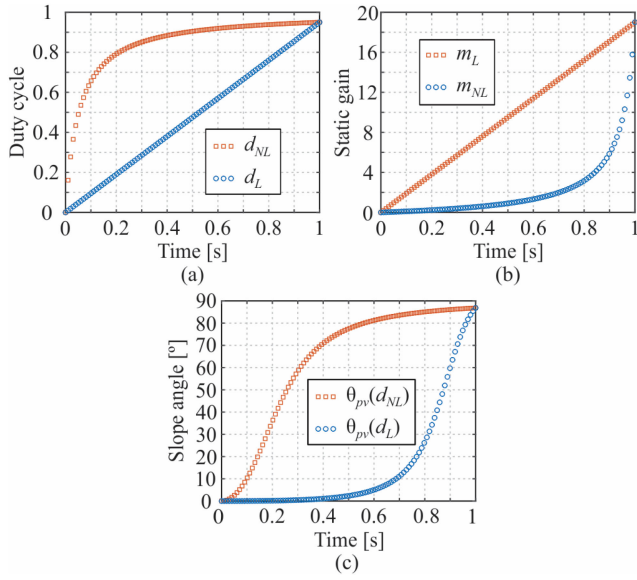
Fig. 3.   (a) Linear and nonlinear duty cycle, (b) linear and nonlinear static gain, and (c) slope angle for both methods considering a resistive load of 20 Ω, sweep time of 1 s, and duty cycle updating on each 10 ms with $D_{max} = 95\%$.
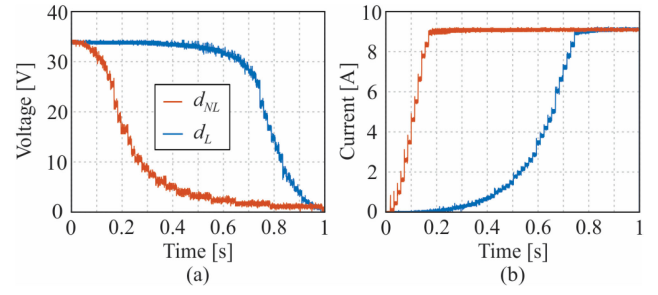

Fig. 4.   Experimental curves for the linear and nonlinear duty cycle update during a complete sweep. (a) Voltage and (b) current of a KB260 PV module.
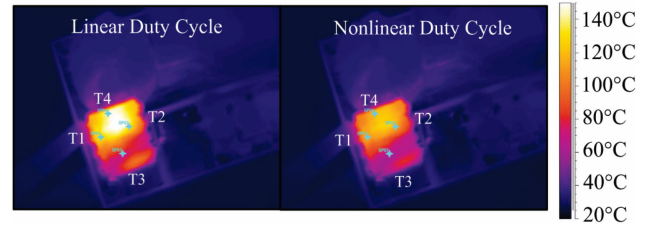

Fig. 5.   Load resistor thermal images under linear and nonlinear duty cycle operation.

was adjusted to $t_{sp} = 1$ s with a duty cycle updating on each 10 ms.

Conventionally, the duty cycle is linearly updated according to (11), implying a nonlinear variation of the static gain, as per (12). However, in this article, it is proposed a different approach, where the converter gain is linearly varied, as stated by (13), and thus, the update of the duty cycle occurs nonlinearly, as in (14). For purposes of comparison, the linear duty cycle d_L, the nonlinear static gain m_{NL}, the nonlinear duty cycle d_{NL}, and the linear static gain m_L are graphically presented in Fig. 3(a) and (b). In the proposed curve tracer, D_{max} is set at 95%, resulting in M_{max} equal to 19, since the relation between D_{max} and M_{max} is given by (15). Because of this choice, the exact value of the short-circuit current cannot be measured, but a very close value can still be obtained.

$$d_L(t) = \frac{D_{max}}{t_{sp}} t \qquad (11)$$

$$m_{NL}(t) = \frac{D_{max} t}{t_{sp} - D_{max} t} \qquad (12)$$

$$m_L(t) = \frac{M_{max}}{t_{sp}} t \qquad (13)$$

$$d_{NL}(t) = \frac{M_{max} t}{t_{sp} + M_{max} t} \qquad (14)$$

$$M_{max} = \frac{D_{max}}{1 - D_{max}} \qquad (15)$$

The variable resistance generated by the dc–dc converter can also be represented in the *I–V* plan as a straight line whose slope angle is given by

$$\theta_{pv} = \tan^{-1}\left(\frac{1}{R_{pv}}\right) = \tan^{-1}\left(\frac{M^2}{R_o}\right) \qquad (16)$$

so that, in order to completely sweep an *I–V* curve, the variable resistance R_{pv} needs to vary from infinite to zero, which means that θ_{pv} should range from 0° to 90°. Fig. 3(c) illustrates the slope angle in both methods for a resistive load of 20 Ω, sweep time of 1 s, and duty cycle updating on each 10 ms.

For a single silicon-based module, the maximum power point is typically localized between 5° and 25°. The linear duty cycle approach may concentrate excessive points in this region, which can cause overheating in the load resistor. Moreover, such approach also concentrates too many points in the voltage source region (close to open-circuit voltage), where less information can be obtained. The nonlinear duty cycle approach shows the opposite: more points in the current source region (close to the short-circuit current). However, more points in this region are important to identify bypass diodes in conduction, which results in steps or notches in *I–V* curve, typically above 30°. Additionally, the number of points close to the maximum power point (MPP) and in voltage source region are sufficient for a more stable and accurate measurement.

As the proposed PV curve tracer is designed to be a portable device, it is also important to reduce the power dissipation in the load resistor, avoiding an excessive internal heating. Thus, an investigation has also been carried out to identify which method is more suitable for the proposed application. Experimental tests were performed to verify its temperature increase during successive sweeps. Fig. 4 shows the voltage and the current of KB260 PV module during one of the sweeps. The temperature evolution was recorded by a thermal camera (FLIR SC600) and depicted in Fig. 5. As expected, when the nonlinear duty cycle is applied, the final temperature in the load resistor is lower, since the time interval in which the PV module operates around the maximum power point is reduced. This condition allows enclosing the
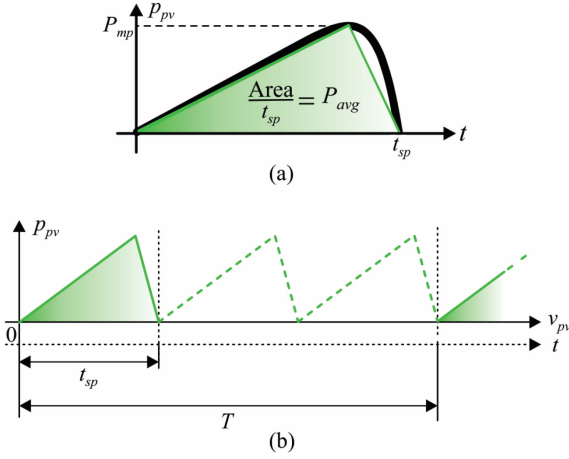
Fig. 6.   (a) Curve approach to calculating P_{avg} and (b) graphical representation of n consecutive sweeps.

Fig. 7.   Photograph of the proposed I–V curve tracer in test.

load resistor in a small hand-held device without damaging it because of overheating. The duty cycle updating time can also be increased to obtain a lower temperature, but this implicates in fewer measured points, which can mask measurement problems.

Another important issue that depends on the control strategy concerns the selection of the load resistor power rating, which should be estimated to allow the complete excursion of the I–V curve between $(0, V_{\text{oc}})$ and $(I_{\text{sc}}, 0)$ without the need for an oversized resistor from the point of view of power dissipation. In fact, an appropriate approach should consider the average power delivered to the load resistor in a sweep period, afterward successive and consecutive scans.

Taking it into account, a methodology is proposed in this article to define the theoretical average power applied in the load in order to find the optimum power rating value for the resistor. Such methodology is based on the principle discussed in the ICC [43], [44], but considering that the P–V curve is used to replace the traditional sinusoidal waveform. In addition, for sake of simplicity, the nonlinear P–V curve is approximated by a triangular shape, as illustrated in Fig. 6(a). Thus, it is possible to define the average power P_{avg} delivered from the PV module to the load in a sweep time t_{sp}, according to

$$P_{\text{avg}} = \frac{1}{t_{sp}} \int_0^{t_{sp}} p_{\text{pv}} dt = \frac{P_{mp}}{2}. \tag{17}$$

Therefore, defining a period T as the time interval in which n consecutive sweeps are performed, the graphic that represents the power in the load resistance is illustrated in Fig. 6(b). Since the PV module deliveries discrete blocks of energy to the load, the relationship between the average power P_{avg} generated by the PV module, in a time interval t_{sp}, and the power P_{Ro} dissipated in the load, during the period T, is given by

$$P_{Ro} = \frac{t_{sp}}{T} P_{\text{avg}} = \frac{t_{sp}}{T} \frac{P_{mp}}{2}. \tag{18}$$

It is important to emphasize that the resistance emulated by the Ćuk converter is limited in the range $[0, \infty]$ independently of the load resistance value, as previously discussed in Table I.
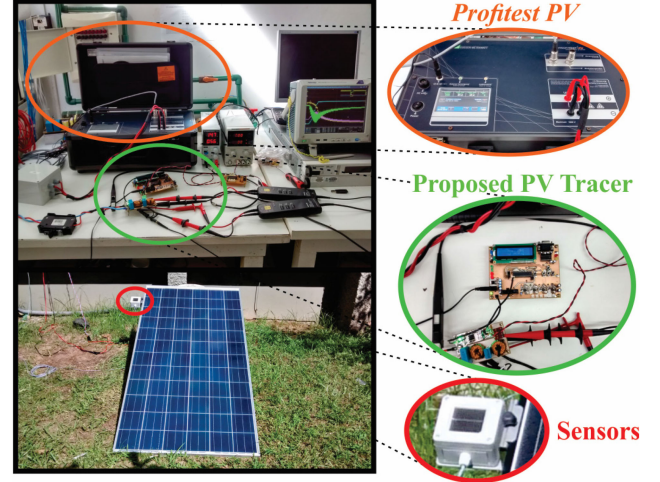
Therefore, ensuring the power dissipation capacity related to the load resistor is higher than P_{Ro}, any resistance can be selected. However, in order to ensure the operation in CCM, the resistance value should satisfy

$$R_o < \frac{2L_iL_of_s}{(L_i + L_o)(1 - D)^2}. \tag{19}$$

In the proposed PV curve tracer, it was assumed a load resistance R_o of 20 Ω with a power rating of 30 W, as a result of a sweep time $t_{sp} = 1$ s, a period $T = 5$ s, and a maximum power $P_{\text{mp}} = 300$ W.

C. Data Acquisition System

The Ćuk converter emulates a resistance whose value is gradually modified by the duty cycle generated by a microcontroller unit (MCU) Atmega328P. During this process, voltage V_{pv}, current I_{pv}, irradiance G, and temperature T are measured, conditioned and accumulated in the RAM of the MCU. The PV module voltage and current are measured by a resistive divider and the ACS724 current sensor, respectively. Conversely, for both irradiance and temperature measurements, it is employed a Z360C irradiation reference sensor, which has also an integrated PT100 temperature sensor. Through the standard RS232 for serial communication, the data is transferred to a computer, evaluated by MATLAB, and presented to the user as the I–V and P–V curves. Furthermore, the points extracted from these experimental curves are used to obtain the five parameters of the electrical equivalent single-diode model [45], enabling the extrapolation of I–V and P–V curves for different values of solar irradiance and temperature.

IV. PRACTICAL EXPERIMENTATION

Fig. 7 shows a photograph of the conducted experimental setup to test the proposed I–V curve tracer for distinct PV modules under different environmental conditions. During the practical experimentation, several tests were performed and
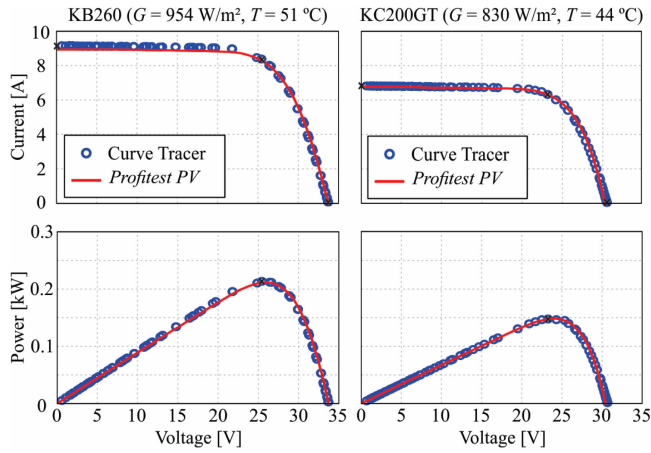
Fig. 8. Experimental *I–V* and *P–V* curves from the KB260 and KC200GT photovoltaic modules.

compared with a commercial PV tracer and data provided by manufacturers.

In order to validate the accuracy of the developed PV curve tracer, its experimental curves were compared with those extracted from the Profitest PV tracer manufactured by the German company Grossen Metrawatt. Fig. 8 illustrates the experimental results obtained considering two distinct modules: KB260 and KC200GT, both from Kyocera. As can be noted, the two devices have presented similar results, with *I–V* and *P–V* curves practically overlapping.

Table IV shows five points for each PV module obtained from the proposed curve tracer and the commercial one, including the open-circuit voltage, the short-circuit current, and the maximum power points. The percent errors between the measurements from the proposed curve tracer and from the Profitest PV (accuracy of 1%) were calculated, demonstrating errors lower than 5%. These errors are mainly related to the employment of a simple signal conditioning circuitry and the usage of an MCU with analog-to-digital converter of only 8 bits, therefore, some straightforward improvements can be made to increase the accuracy of the device. In addition, since the curves were not simultaneously measured by the devices, small deviations can be justified by slight changes in the weather conditions. Errors of the additional points were not estimated because they may not correspond to the same operating points.

Fig. 9 presents the short-circuit current, the open-circuit voltage, and the maximum power of the modules as function of temperature, for constant solar irradiance. As can be seen, the temperature has a slight effect in I_{sc}, but its increase results in a linear reduction in V_{oc} and P_{mp}. Table V compares the calculated thermal coefficients values using the experimental results and the manufacturer data. In general, the temperature coefficients β (of V_{oc}) and γ (of P_{mp}) are in good agreement with their datasheets. In contrast, because of its low value, the coefficient α (of I_{sc}) has demonstrated a great deviation from datasheet.

Fig. 10 shows a similar analysis to evaluate the effect of solar irradiance on the curves of PV modules. The experimental values of I_{sc}, V_{oc}, and P_{mp} are plotted as function of irradiance, for

TABLE IV
MEASURED ELECTRICAL QUANTITIES FROM THE PV MODULES

PV Module		Reference (Profitest PV)	Measured (Proposed one)	|Error| (%)
KC200GT	V_{mp}	24.26 V	23.28 V	4.03
	I_{mp}	6.01 A	6.23 A	3.66
	V_{oc}	30.47 V	30.78 V	1.02
	I_{sc}	6.77 A	6.82 A	0.74
	V_4	9.77 V	9.78 V	-
	I_4	6.72 A	6.77 A	-
	V_5	28.71 V	28.67 V	-
	I_5	3.00 A	2.93 A	-
KB260	V_{mp}	25.70 V	25.44 V	1.00
	I_{mp}	8.23 A	8.38 A	1.82
	V_{oc}	33.76 V	33.77 V	0.03
	I_{sc}	8.93 A	9.15 A	2.46
	V_4	9.90 V	9.59 V	-
	I_4	8.90 A	9.12 A	-
	V_5	31.40 V	31.31 V	-
	I_5	3.87 A	3.81 A	-
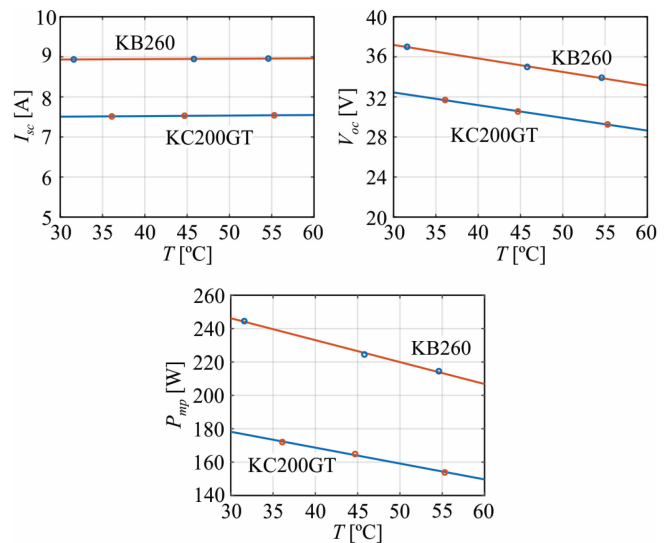
Fig. 9. Experimental results of I_{sc}, V_{oc}, and P_{mp} as function of temperature T for KB260 ($G \approx 960$ W/m^2) and KC200GT ($G \approx 925$ W/m^2) PV modules.

TABLE V
MEASURED THERMAL COEFFICIENT VALUES

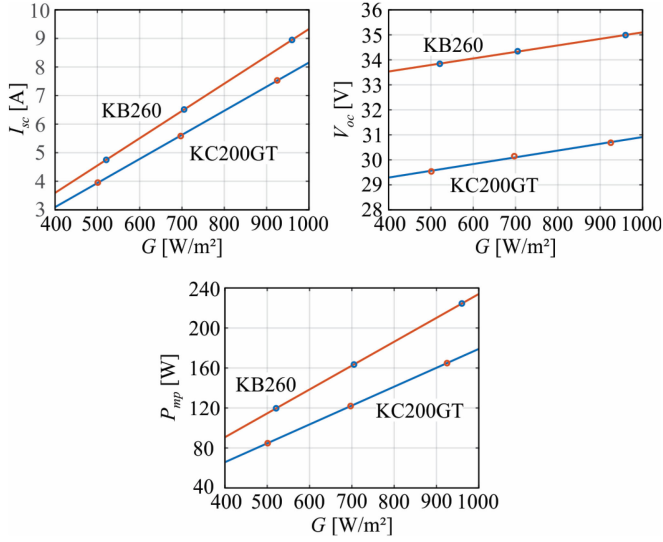|	KC200GT		KB260	
	Calculated	Datasheet	Calculated	Datasheet
α [%/°C]	0.017	0.04	0.010	0.06
β [%/°C]	-0.386	-0.37	-0.352	-0.36
γ [%/°C]	-0.476	n/a	-0.506	-0.45

Fig. 10.   Experimental results of I_{sc}, V_{oc}, and P_{mp} as function of irradiance G for KB260 ($T \approx 46$ °C) and KC200GT ($T \approx 45$ °C) PV modules.

Fig. 11.   (a) I–V curve shape variation for impairment according to IEC 62446-1. (b) Comparison between I–V curves from two single-diode models considering the experimental measurements and the data provided by manufacturer at STC.

TABLE VI
SINGLE-DIODE MODEL ELECTRICAL PARAMETERS

Parameter	KC200GT	KB260
Photogenerated current ($I_{ph,ref}$)	6.84 A	9.16 A
Saturation current ($I_{s,ref}$)	238.21 nA	854.46 nA
Ideality factor (A)	1.22	1.24
Series resistance (R_s)	6.83 mΩ	5.78 mΩ
Shunt resistance (R_{sh})	3.08 Ω	4.45 Ω

TABLE VII
COMPARISON WITH COMMERCIAL DEVICES

Model	I-V range	Sweep time	Weight	Cost
Proposed PV tracer	50 V; 10 A	1 s	0.35 kg	$265.00*
Amprobe Solar-600	60 V; 12 A	0 - 3 s	1.16 kg	$2,299.95
EKO MP-11	1000 V; 30 A	0 - 5 s	3.0 kg	n/a
HT I-V500w	1500 V; 15 A	n/a	1.2 kg	$4,495.00
Seaward PV210	1000 V; 15 A	n/a	1.04 kg	$2,595.00
Solmetric PVA-1000S	1000 V; 20 A	0.05 - 2 s	n/a	$5,695.00

*Irradiance sensor is not included.

constant temperature. As irradiance increases, all the variables also increase so that V_{oc} has a lower increasing rate than I_{sc} and P_{mp}. However, it clearly demonstrates that the solar irradiance has a larger impact on V_{oc} than the temperature has over I_{sc}. Such results are in agreement with results reported in datasheets and other works [1], [2].

From the points (I_{pv}, V_{pv}) presented in Table IV it was possible to find the five parameters related to the single-diode model, for each tested PV module. For this purpose, a nonlinear least square algorithm able to solve a five equations nonlinear system was developed in MATLAB [45]. The obtained parameters are shown in Table VI and can be used to extrapolate the curves for any other irradiance and temperature conditions.

When compared with the data from manufacturers, they can provide information about any impairment that reduces the output power of PV modules. The IEC 62446-1 classifies six I–V curve shape variations for impairments signatures, as illustrated in Fig. 11(a), which helps to identify their nature. These shapes are known as: 1) steps or notches; 2) low current; 3) low voltage; 4) rounder knee; 5) shallower slope in voltage source region; and 6) steeper slope in current source region [10].

For example, Fig. 11(b) depicts the I–V curves of two single-diode models at STC: the first concerned to the tested KB260
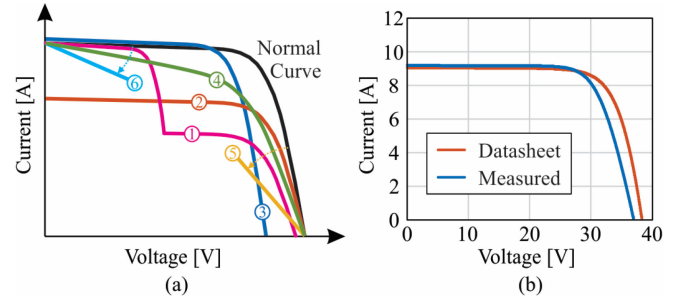
module (see Table VI) and other one obtained from data provided by the manufacturer. In this case, one can identify the low voltage signature, which may indicate shorted bypass diodes, but more probably potential-induced degradation, caused by leakage currents [46]. A slight lower slope in the voltage source region can also be noted, indicating an increase in the series resistance of the PV module. Certain degradation mechanisms are able to increase it, as corrosion of metal terminals in the module connectors or on the interconnects between cells [47].

V. COMPARISON WITH COMMERCIAL DEVICES

The proposed PV curve tracer was compared with some commercial portable devices in terms of measurement range, sweep time, weight, and cost, as described in Table VII. This information was obtained from websites and datasheets from manufacturers. For the comparison, the proposed PV curve tracer has been redesigned to become a hand-held device, as demonstrated in Fig. 12. In general, the commercial portable I–V tracers use the capacitor load method. In such method, the sweep speed depends on the charging time, with a maximum time varying between 2 to 5 s. Moreover, they also need high-quality, heavy capacitors, making them heavier and more expensive than the dc–dc converter method. Despite they are typically designed to also measure PV strings, the Amprobe Solar-600 (that presents a similar I–V range) is three times heavier than

Fig. 12. Practical realization of the hand-held PV curve tracer—dimensions: a 100×220 mm (L × C) and weight equal to 0.35 kg.

the proposed design with a dc–dc Ćuk converter. The partial cost of the proposed device was estimated in $265/unit. This value accounts all the components employed to assemble the device, but the employed Z360C irradiation reference sensor has not been included. Additionally, it should be mentioned that such price is valid for manufacturing only one unit, in a scale production it will be probably reduced.

It is worth mentioning that the dc–dc converter method can also be extended to measure *I–V* curves of PV strings. However, two main issues should be taken into account when designing it. The first one is how to deal with the high input voltage, since it affects the selection of semiconductor devices current available in the market. The second problem concerns to the high power, which may limit the employment of conventional dc–dc converters. To overcome these issues, a simple solution, for example, would be the usage of a step-down switched-capacitor dc–dc converter [48] with a fixed and noncontrollable static gain in the first stage followed by an interleaved Ćuk converter [49]. Another solution would be the use of Flyback converters in an input-series output-parallel configuration [50]. Both solutions can implement interleaving techniques, which considerably increases the apparent frequency in most passive components, making it possible to reduce them.

VI. Conclusion

This article has presented a design methodology to develop a low-cost, portable PV *I–V* curve tracer, based on the usage of a dc–dc Ćuk converter, for modules of up to 300 W. In order to obtain a compact, low-cost device, some design techniques have been proposed, such as: circuit reduction, high switching frequency operation, nonlinear duty cycle variation, and the employment of ICC for sequential measurements. The proposed PV tracer has been tested in real conditions and its results have been compared with a commercial device. It has demonstrated satisfactory accuracy even with simple signal conditioning circuitry and low-cost, low-resolution MCU. The obtained results were used to extract the single-diode models of the tested PV modules. As a result, by applying these models, it was possible to compare the actual characteristics of the modules with data provided by manufacturers, helping to identity aging processes. Finally, when compared with commercial portable devices based

on the capacitive load method, the proposed *I–V* curve tracer presents lower cost and lower weight, demonstrating that the dc–dc converter method can represent a future trend in *I–V* tracers.

References

[1] M. D. Yandt, J. P. D. Cook, M. Kelly, H. Schriemer, and K. Hinzer, "Dynamic real-time I-V curve measurement system for indoor/outdoor characterization of photovoltaic cells and modules," *IEEE J. Photovolt.*, vol. 5, no. 1, pp. 337–343, Jan. 2015.

[2] M. G. Villalva, J. R. Gazoli, and E. R. Filho, "Comprehensive approach to modeling and simulation of photovoltaic arrays," *IEEE Trans. Power Electron.*, vol. 24, no. 5, pp. 1198–1208, May 2009.

[3] *Photovoltaic Devices - Procedures for Temperature and Irradiance Corrections to Measured I-V Characteristics*, IEC Standard 60891, 2009.

[4] *Photovoltaic Devices - Part 1: Measurement Of Photovoltaic Current-Voltage Characteristics*, IEC Standard 60904-1:2006, 2006.

[5] *Photovoltaic (PV) Systems - Requirements for Testing, Documentation and Maintenance - Part 1: Grid Connected Systems - Documentation, Commissioning Tests and Inspection*, IEC Standard 62446-1:2018, 2018.

[6] *Photovoltaic (PV) Array - On-Site Measurement of Current-Voltage Characteristics*, IEC Standard 61829:2015, 2015.

[7] F. Bradaschia, M. C. Cavalcanti, A. J. Nascimento, Jr., E. A. Silva, and G. M. S. Azevedo, "Parameter identification for PV modules based on environment-dependent double-diode model," *IEEE J. Photovolt.*, vol. 9, no. 5, pp. 1388–1397, Sep. 2019.

[8] E. A. Silva, F. Bradaschia, M. C. Cavalcanti, and A. J. Nascimento, "Parameter estimation method to improve the accuracy of photovoltaic electrical model," *IEEE J. Photovolt.*, vol. 6, no. 1, pp. 278–285, Jan. 2016.

[9] E. Duran *et al.*, "Different methods to obtain the I-V curve of PV modules: A review," in *Proc. Photovolt. Specialists Conf.*, 2008. pp. 1–6.

[10] Y. Zhu and W. Xiao, "A comprehensive review of topologies for photovoltaic I-V curve tracer," *Sol. Energy*, vol. 196, pp. 346–357, Jan. 2020.

[11] H. Amiry *et al.*, "Design and implementation of a photovoltaic I-V curve tracer: Solar modules characterization under real operation conditions," *Energy Convers. Manage.*, vol. 169, pp. 206–216, Aug. 2018.

[12] A. E. Hammoumi, S. Motahhir, A. Chalh, A. E. Ghzizal, and A. Derouich, "Low-cost virtual instrumentation of PV panel characteristics using Excel and Arduino in comparison with tradition instrumentation," *Renewables: Wind, Water, Sol.*, vol. 5, pp. 1–16, Mar. 2018.

[13] A. Rivai and N. A. Rahim, "Binary-based tracer of photovoltaic array characteristics," *IET Renewable Power Gener.*, vol. 8, no. 6, pp. 621–628, Aug. 2014.

[14] E. E. van Dyk, A. R. Gxasheka, and E. L. Meyer, "Monitoring current-voltage characteristics and energy output of silicon photovoltaic modules," *Renewable Energy*, vol. 30, pp. 399–411, 2005.

[15] Z. Chen *et al.*, "A capacitor based fast I-V characteristics tester for photovoltaic," *Energy Procedia*, vol. 145, pp. 381–387, Apr. 2018.

[16] R. G.-Valverde *et al.*, "Portable and wireless IV-curve tracer for >5 kW organic photovoltaic modules," *Sol. Energy Mater. Sol. Cells*, vol. 151, pp. 60–65, Jul. 2016.

[17] J. Muñoz and E. Lorenzo, "Capacitive load based on IGBTs for on-site characterization of PV arrays," *Sol. Energy*, vol. 80, pp. 1489–1497, 2006.

[18] H. M. Aguilar, R. F. Maldonado, and L. B. Navarro, "Charging a capacitor with a photovoltaic module," *Phys. Educ.*, vol. 52, no. 4, pp. 1–4, May 2017.

[19] F. Spertino, J. Sumaili, H. Andrei, and G. Chicco, "PV module parameter characterization from transient charge of an external capacitor" *IEEE J. Photovolt.*, vol. 3, no. 4, pp. 1325–1333, Oct. 2013.

[20] M. M. Mahmoud, "Transient analysis of a PV power generator charging a capacitor for measurement of the I-V characteristics" *Renewable Energy*, vol. 31, pp. 2198–2206, 2006.

[21] F. Spertino *et al.*, "Capacitor charging method for I–V curve tracer and MPPT in photovoltaic systems," *Sol. Energy*, vol. 119, pp. 461–473, 2015.

[22] P. Papageorgas *et al.*, "A low cost and fast PV I-V curve tracer based on an open source platform with M2M communication capabilities for preventive monitoring," *Energy Procedia*, vol. 74, pp. 423–438, Aug. 2015.

[23] Y. Kuai and S. Yuvarajan, "An electronic load for testing photovoltaic panels," *J. Power Sources*, vol. 154, pp. 308–313, 2006.

[24] V. Leite, J. Batista, F. Chenlo, and J. L. Afonso, "Low-cost instrument for tracing current-voltage characteristics of photovoltaic modules," *Renewable Energy Power Qual. J.*, vol. 1, no. 10, pp. 1012–1017, 2012.

[25] A. Sahbel, N. Hassan, M. M. Abdelhameed, and A. Zekry, "Experimental performance characterization of photovoltaic modules using DAQ," *Energy Procedia*, vol. 36, pp. 323–332, 2013.

[26] A. A. Willoughby and M. O. Osinowo, "Development of an electronic load I-V curve tracer to investigate the impact of Harmattan aerosol loading on PV module pern2tkformance in Southwest Nigeria," *Sol. Energy*, vol. 166, pp. 171–180, 2018.

[27] O. Henni, M. Belarbi, K. Haddouche, and E.-H. Belarbi, "Design and implementation of a low-cost characterization system for photovoltaic solar panels," *Int. J. Renewable Energy Res.*, vol. 7, no. 4, pp. 1586–1594, 2017.

[28] E. D. Aranda, J. A. G. Galan, M. S. Cardona, and J. M. A. Marquez, "Measuring the I-V curve of PV generators," *IEEE Ind. Electron. Mag.*, vol. 3, no. 3, pp. 4–14, Sep. 2009.

[29] E. Durán, J. M. Andújar, J. M. Enrique, and J. M. Pérez-Oria, "Determination of PV generator I-V/P-V characteristic curves using a DC-DC converter controlled by a virtual instrument," *Int. J. Photoenergy*, vol. 2012, 2012, Article no. 843185.

[30] E. Durán, J. Galán, J. M. Andujar, and M. S. Cardona, "A new method to obtain I-V characteristics curves of photovoltaic modules based on SEPIC and Cuk converters," *EPE J.*, vol. 18, no. 2, pp. 5–15, Jun. 2008.

[31] C. W. Riley, "An autonomous online I-V tracer for PV monitoring applications," Master's thesis, Dept. Elect. Eng., Univ. Tennessee, Knoxville, TN, USA, 2014.

[32] I. F. Silva, P. S. Vicente, F. L. Tofoli, and E. M. Vicente, "Portable and low cost photovoltaic curver tracer," in *Proc. IEEE Brazilian Power Electron. Conf.*, 2017, pp. 1–6.

[33] T. Khatib, W. Elmenreich, and A. Mohamed, "Simplified I-V characteristic tester for photovoltaic modules using a DC-DC boost converter," *Sustainability*, vol. 9, no. 657, pp. 1–12, 2017.

[34] N. N. Lima *et al.*, "Low complexity system for real-time determination of current-voltage characteristic of PV modules and strings," in *Proc. IEEE Appl. Power Electron. Conf.*, 2013, pp. 2817–2823.

[35] T. A. Pereira *et al.*, "Electrical characterizer of photovoltaic modules using the DC/DC Ćuk converter," in *Proc. IEEE Int. Conf. Ind. Technol.*, 2018, pp. 954–959.

[36] R. F. Coelho, F. M. Concer, and D. C. Martins, "A study of the basic DC-DC converters applied in maximum power pointing tracking," in *Proc. IEEE Brazilian Power Electron. Conf.*, 2009, pp. 673–678.

[37] R. F. Coelho, F. M. Concer, and D. C. Martins, "Analytical and experimental analysis of DC-DC converters in photovoltaic maximum power point tracking applications," in *Proc. IEEE Ind. Electron. Soc. Conf.*, 2010, pp. 2778–2783.

[38] A. Safari and S. Mekhilef, "Simulation and hardware implementation of incremental conductance MPPT with direct control method using Cuk converter," *IEEE Trans. Ind. Electron.*, vol. 58, no. 4, pp. 1154–1161, Apr. 2011.

[39] S. Dian, X. Wen, X. Deng, and S. Zhang, "Digital control of isolated Cuk power factor correction converter under wide range of load variation," *IET Power Electron.*, vol. 8, no. 1, pp. 142–150, Jan. 2015.

[40] E. Babaei and M. E. S. Mahmoodieh, "Systematical method of designing the elements of the Cuk converter," *Elect. Power Energy Syst.*, vol. 55, pp. 351–361, 2014.

[41] M. J. Reno and C. W. Hansen, "Identification of periods of clear sky irradiance in time series of GHI measurements," *Renewable Energy*, vol. 90, pp. 520–531, 2016.

[42] H. Schmidt, B. Burger, U. Bussemas, and S. Elies, "How fast does an MPP tracker really need to be?," in *Proc. 24th Eur. Photovolt. Energy Sol. Conf.*, 2009, pp. 3273–3276.

[43] Y. N. Chang, G. T. Heydt, and Y. Liu, "The impact of switching strategies on power quality for integral cycle controllers," *IEEE Trans. Power Del.*, vol. 18, no. 3, pp. 1073–1078, Jul. 2003.

[44] C. V. V. Reddy, R. D. Kulkarni, P. Rautela, and M. Salim, "Design and simulation of integral cycle control based thyristor controller for power quality improvement," in *Proc. Int. Conf. Convergence Technol.*, 2018, pp. 1–6.

[45] B. K. Nayak, A. Mohapatra, and K. B. Mohanty, "Parameters estimation of photovoltaic module using nonlinear least square algorithm: A comparative study," in *Proc. IEEE India Conf.*, 2013, pp. 1–6.

[46] P. Hacke *et al.*, "Accelerated testing and modelling of potential-induced degradation as function of temperature and relative humidity," *IEEE J. Photovolt.*, vol. 5, no. 6, pp. 1549–1553, Nov. 2015.

[47] E. L. Meyer and E. E. van Dyk, "Assessing the realiability and degradation of photovoltaic module performance parameters," *IEEE Trans. Rel.*, vol. 53, no. 1, pp. 83–92, Mar. 2004.

[48] M. D. Seeman and S. R. Sanders, "Analysis and optimization of switched-capacitor DC-DC converters," *IEEE Trans. Power Electron.*, vol. 23, no. 2, pp. 841–851, Mar. 2008.

[49] K. D. Joseph, A. E. Daniel, and A. Unnikrishnan, "Interleaved Cuk converter with improved transient performance and reduced current ripple" *J. Eng.*, vol. 2017, no. 7, pp. 362–369, Jul. 2017.

[50] A. Rodriguez *et al.*, "Auxiliary power supply based on a modular ISOP flyback configuration with very high input voltage," in *Proc. IEEE Energy Convers. Congr. Expo.*, 2016, pp. 1–7.